Available online at www.sciencedirect.com

ScienceDirect

Procedia Structural Integrity 45 (2023) 132–139

Structural Integrity Procedia

www.elsevier.com/locate/procedia

17th Asia-Pacific Conference on Fracture and Strength and the 13th Conference on Structural Integrity and Failure (APCFS 2022 & SIF 2022)

Vibrations of axially travelling CNT reinforced beams with clamped-clamped boundary condition and an elastic support

Moaz Sibtain[a,*], Saxon Smith[a], Alireza Yeganehmehr[b], Oscar Zi Shao Ong[a] and Mergen H. Ghayesh[a]

[a]*School of Electrical and Mechanical Engineering, The University of Adelaide, Adelaide, SA 5005, Australia*
[b]*School of Architecture and Civil Engineering, The University of Adelaide, Adelaide, SA 5005, Australia*

Abstract

Vibrational analysis in engineering systems of axially travelling beams has attracted noticeable attention due to the many applications, such as in robotic manipulators, cable tramways, textile fibres, and in general when there is the axial mass transport of a continuous structure. This article studies the vibrational response of axially-travelling, functionally-graded, carbon nanotube-(CNT)-reinforced beam structures, by investigating linear gyroscopic aspects, such as Argand diagrams. The distribution of CNT fibres is assumed to vary along the thickness of the beam. The Hamilton principle is employed to obtain the coupled axial and transverse behaviour of the beam, subjected to clamped-clamped boundary condition and additionally supported by a spring. These equations of motion are then solved using the modal decomposition technique for the Coriolis-dependent axial and transverse frequencies. For verification, the results are compared to the simplified case in the literature for CNT strengthened beams with zero axial velocity, the dynamics of axially travelling beams, studies of the clamped-clamped boundary condition, and the effects on the Argand diagrams, which have been performed. The Argand diagrams are plotted to examine the effects of varying axial speed on the different linear characteristics of vibration. Variation of the volume fraction of the CNT and the spring support, has also been considered, to understand its effects on the vibration characteristics. Results produced in this article are important in assisting in the future design of engineering devices involving axially travelling systems.

Keywords: Argand diagrams; axially travelling; CNT reinforced beam; Hamilton's principle.

* Corresponding author. Tel.: +61 415 449 366
E-mail address: moaz.sibtain@adelaide.edu.au

2452-3216
10.1016/j.prostr.2023.05.006

1. Introduction

Carbon nanotubes (CNTs) have attracted substantial attention since their inception in the early 1990s for their mechanical properties Iijima et al. (1993), such as thermal and electrical conductivity, low density and high strength, with a Young's modulus of 1 TPa Shirasu et al. (2017). These characteristics can be varied by the chirality and diameter of the CNT, to optimise these properties for a specific application. Due to their extraordinary properties, they make an excellent candidate as a reinforcement to current materials Popov et al. (2004). This paper investigates the dynamics of a CNT reinforced axially travelling beam with intermediate spring support.

1.1. Functionally graded CNT reinforcement

There is interest in new reinforcements that can improve mechanical properties to the matrix without adding as much weight to the material Drissi-Habti et al. (2021). Materials with a functionally graded reinforcement have a variation in the composition of the reinforcement structure along the cross section. Specifically, FGCNT reinforcement can produce beneficial properties Zhai et al. (2021). Utilising FGCNT reinforcement can maximise the size of the wind turbine blades expanding potential energy extraction at a given wind farm location Zafar (2018).

Due to the exciting properties mentioned above and the wide variety of the applications, many papers have been written on carbon nanotubes being functionally graded for CNT reinforcement Liew et al. (2015) & Khaniki (2022). An exceptional use is the tailoring of the material for the application, as different forms of FGCNT reinforcement allow for an altering of the natural frequency of the matrix, which can reduce harmonic resonance at critical operational ranges Ansari et al. (2019) & Öz et al. (1999).

1.2. Applications of axially travelling beams

There are a wide variety of applications of axially travelling beams; for instance, food processing with roller-to-roller systems, electronic printed flexible membranes, medical nano-robots, railway contact wires, and conveyor belts Dahlberg et al. (2006). It is important to analyse the vibrational characteristics to avoid resonance, and hence wear and damage Poornima (2021).

In these systems investigated, velocities have effects on the natural frequency Öz et al. (1999) and Pakdemirli (1997). Understanding the critical velocities of the system is important, to ascertain if the operational speed of the systems will induce undesired harmonic motion, as mechanical systems work under tight tolerances Swanson (2005). Understanding the effects on these said systems will increase the service life of those machines. For systems with lower original speeds, the chance of supercritical vibrations and hence complex dynamics, such as chaos, is larger Ravindra (1998). Farokhi and Ghayesh (2016) examined what effect vibrations in lateral, transverse and longitudinal directions had on axially travelling beams. It was concluded that increasing the velocity of the axially travelling beam does not necessarily increase the possibility of chaotic motion Yang (2005) & Pellicano (2002).

1.3. Axially travelling functionally graded CNT reinforced beams

A number of papers deal with this area. For example, it was found that an increase in velocity increases the variation of amplitude of vibration, resulting in misalignment and imbalance around the centre of rotation, leading to premature wear to a system Yan (2020). It is shown that adding FGCNT reinforcement to a beam increases the natural frequency Mohammadimehr et al. (2020) & Ong (2022).

The aim of this paper is to examine the dynamics of axially travelling FGCNT reinforced beams, with an intermediate spring support on the beam; in other words, this paper aims at analysing the linear vibration characteristics of CNT reinforced beams subject to an axial speed (which generates Coriolis terms). Understanding these properties is critical to ensuring future materials manufactured with these functionally graded reinforcements are robust and meet "fit for purpose" industrial applications, where a reduction of wear and fracture in industry is key to sustaining long asset service life. This paper looks at a polymethyl methacrylate matrix with FGCNT reinforcement. Different volume fractions and spring stiffness were analysed to understand what effect this has on the vibrational properties of the beam. This is followed by analysis on increasing the velocity of the beam and how this affects the natural frequency.

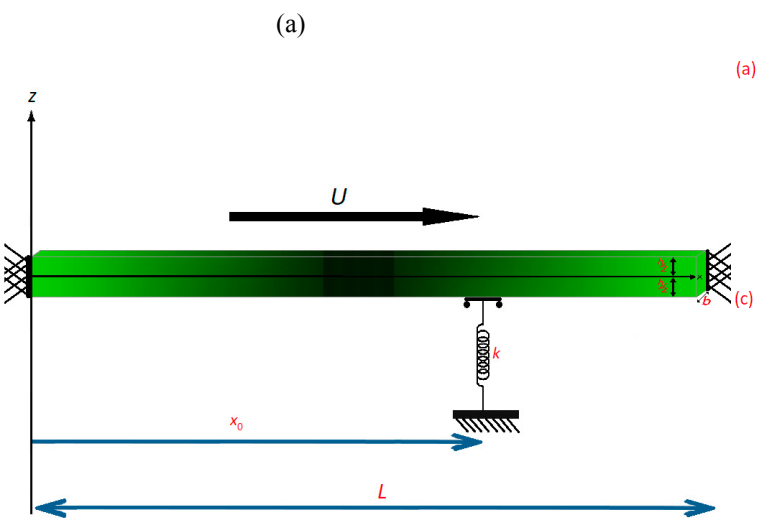

Fig. 1. (a): Clamped-clamped axially travelling beam with varying velocities, U, where k is the spring support, x_0 is the location of the spring, b is the width of the beam and h is the height of the FGCNT reinforced beam.

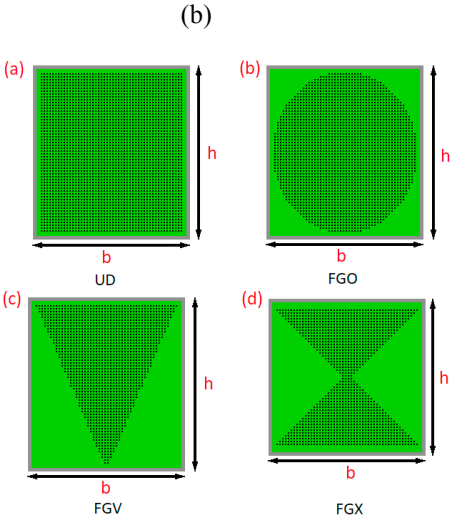

Fig. 1. (b): The four different configuration of CNT: of the FGCNT reinforced beam (a) UD; (b) FG-O; (c) FG-V; (d) FG-X along the width and height.

Fig. 1. (a) shows the axially travelling CNT reinforced beam under clamped-clamped boundary condition, with an elastic support. Fig. 1. (b) is a cross-sectional view of these axially travelling beams displaying their respective CNT reinforcement.

2. Axially travelling CNT reinforced beam model

The following equations describes the material properties of the FGCNT reinforced beam according to the rule of mixture Wattanasakulpong et al. (2015)

$$\rho_r(z) = (\rho_{SW} - \rho_m) V_{SW}(z) + \rho_m, \tag{1}$$

$$E_r(z) = (c_1 E_{SW} - E_m) V_{SW}(z) + E_m, \tag{2}$$

where c_1 is the CNT efficiency parameter, subscripts m and SW represents the matrix, and single-walled carbon nanotube (SWCNT), respectively. The volume fraction is represented by V .

The volume fraction of the matrix is

$$V_m(z) = 1 - V_{SW}(z). \tag{3}$$

The following functions represent the different types of CNT distribution models for FGCNT reinforced beam Thomas (2016):

$$V_{SW}(z) = \begin{cases} V_{SW}^* & \text{(Uniformly distributed)}, \\ \left(1 + \dfrac{2z}{h}\right) V_{SW}^* & \text{(FG-V)}, \\ 2\left(1 - \dfrac{2|z|}{h}\right) V_{SW}^* & \text{(FG-O)}, \\ \dfrac{4|z|}{h} V_{SW}^* & \text{(FG-X)}. \end{cases} \tag{4}$$

where ρ_m and ρ_{SW} are the densities of matrix and CNT, respectively.

Based on the Euler-Bernoulli beam theory, the non-zero, linear strain and stress components are

$$\varepsilon_{xx} = \frac{\partial v_x(x,t)}{\partial x} - z\frac{\partial^2 v_y(x,t)}{\partial x^2}, \tag{5}$$

$$\sigma_{xx} = \frac{E_r(z)}{1-\nu^2}\left[\frac{\partial v_x(x,t)}{\partial x} - z\frac{\partial^2 v_y(x,t)}{\partial x^2}\right], \tag{6}$$

where v_x and v_y denotes axial and transverse displacements, respectively, and z is in the thickness direction, as shown in Fig. 1, and E_r is the Young's modulus of the FGCNT reinforced beam.

The kinetic energy (K_E) of the system (possess terms related to the axial speed) is

$$K_E = \frac{1}{2}\int_0^L \rho_r(z)\left[\left(\frac{\partial v_x(x,t)}{\partial t} + U\left(\frac{\partial v_x(x,t)}{\partial x}+1\right)\right)^2 + \left(\frac{\partial v_y(x,t)}{\partial t} + U\frac{\partial v_y(x,t)}{\partial x}\right)^2\right] dAdx, \tag{7}$$

The potential energy (π_t) of system is the sum of the strain energy (π_E) and the spring stiffness energy (π_s) in which k is the elastic spring stiffness. The following dimensionless parameters were introduced:

$$v_y^* = \frac{v_y}{h},\ v_x^* = \frac{v_x}{h},\ x^* = \frac{x}{L},\ x_0^* = \frac{x_0}{L},\ z^* = \frac{z}{h},\ \lambda = \sqrt{\frac{L}{h}},\ t^* = t\sqrt{\frac{A_{3,m}}{I_{xx,m}L^4}}$$

$$A_1^* = \frac{A_1 h^2}{A_{3,m}},\ A_2^* = \frac{A_2 h}{A_{3,m}},\ A_3^* = \frac{A_3}{A_{3,m}},\ I_{xx}^* = \frac{I_{xx}}{I_{xx,m}},\ k^* = \frac{kL^3}{A_{3,m}},\ c = U\sqrt{\frac{I_{xx,m}L^2}{A_{3,m}}}, \tag{8}$$

where h denotes the beam's thickness, and the subscript m represents the matrix's material properties.

By using the generalised Hamilton principle, the following dimensionless equations of motion are determined:

$$-\lambda^4\frac{\partial}{\partial x}\left\{A_1\left(\frac{\partial v_x(x,t)}{\partial x}\right)\right\} + \lambda^2\frac{\partial}{\partial x}\left\{A_2\left(\frac{\partial^2 v_y(x,t)}{\partial x^2}\right)\right\}$$
$$+I_{xx}(z)\left[\left(\frac{\partial^2 v_x(x,t)}{\partial t^2}\right) + 2c\left(\frac{\partial^2 v_x(x,t)}{\partial x\partial t}\right) + c^2\left(\frac{\partial^2 v_x(x,t)}{\partial x^2}\right)\right] = 0, \tag{9}$$

$$\lambda^2\frac{\partial^2}{\partial x^2}\left\{A_2\left(\frac{\partial v_x(x,t)}{\partial x}\right)\right\} + \frac{\partial^2}{\partial x^2}\left\{A_3\left(\frac{\partial^2 v_y(x,t)}{\partial x^2}\right)\right\}$$
$$+I_{xx}\left[\left(\frac{\partial^2 v_y(x,t)}{\partial t^2}\right) + 2c\left(\frac{\partial^2 v_y(x,t)}{\partial x\partial t}\right) + c^2\left(\frac{\partial^2 v_y(x,t)}{\partial x^2}\right)\right] + kv_y\delta(x-x_0) = 0, \tag{10}$$

where star notation is dropped for simplicity.

where I_{xx} is a coefficient that denotes the mass moment of inertia

$$I_{xx} = \int_A \left[(\rho_{SW}-\rho_m)V_{SW}(z) + \rho_m\right] dA. \tag{11}$$

and A_1, A_2, and A_3 are stiffness parameters and are defined as

$$\{A_1, A_2, A_3\} = \int_A \left[(c_1E_{SW} - E_m)V_{SW}(z) + E_m\right]\{1, z, z^2\}\, dA, \tag{12}$$

3. Solution method

The modal decomposition technique was used in order to solve the coupled dimensionless equation of motion; more details for general form of this method for a system of equations of motion is depicted in Zhai et al. (2021).

By employing the modal decomposition method (as a sub-class of an assumed-mode technique), the axial and transverse vibration frequencies of the axially travelling FGCNT reinforced beam with an intermediate spring support are determined.

4. Results and discussion

The CNT reinforced beam is modelled as a polymer with CNT fibres reinforced in a PMMA matrix. The material properties for the matrix and the CNT reinforcement used to generate the numerical results in this paper are: $\rho_m = 1150$ kg/m^3, $E_m = 2.9$ GPa , $E_{SW} = 869$ GPa, $\rho_{SW} = 1740$ kg/m^3. The geometric properties of the beam are: length, $L = 2$ m, and height, $h = 0.1$ m. Three different CNT volume fractions were considered in this paper which are 0.11, 0.14 and 0.28, with the CNT efficiency parameters of 0.149, 0.150 and 0.141, respectively Daikh et al. (2021).

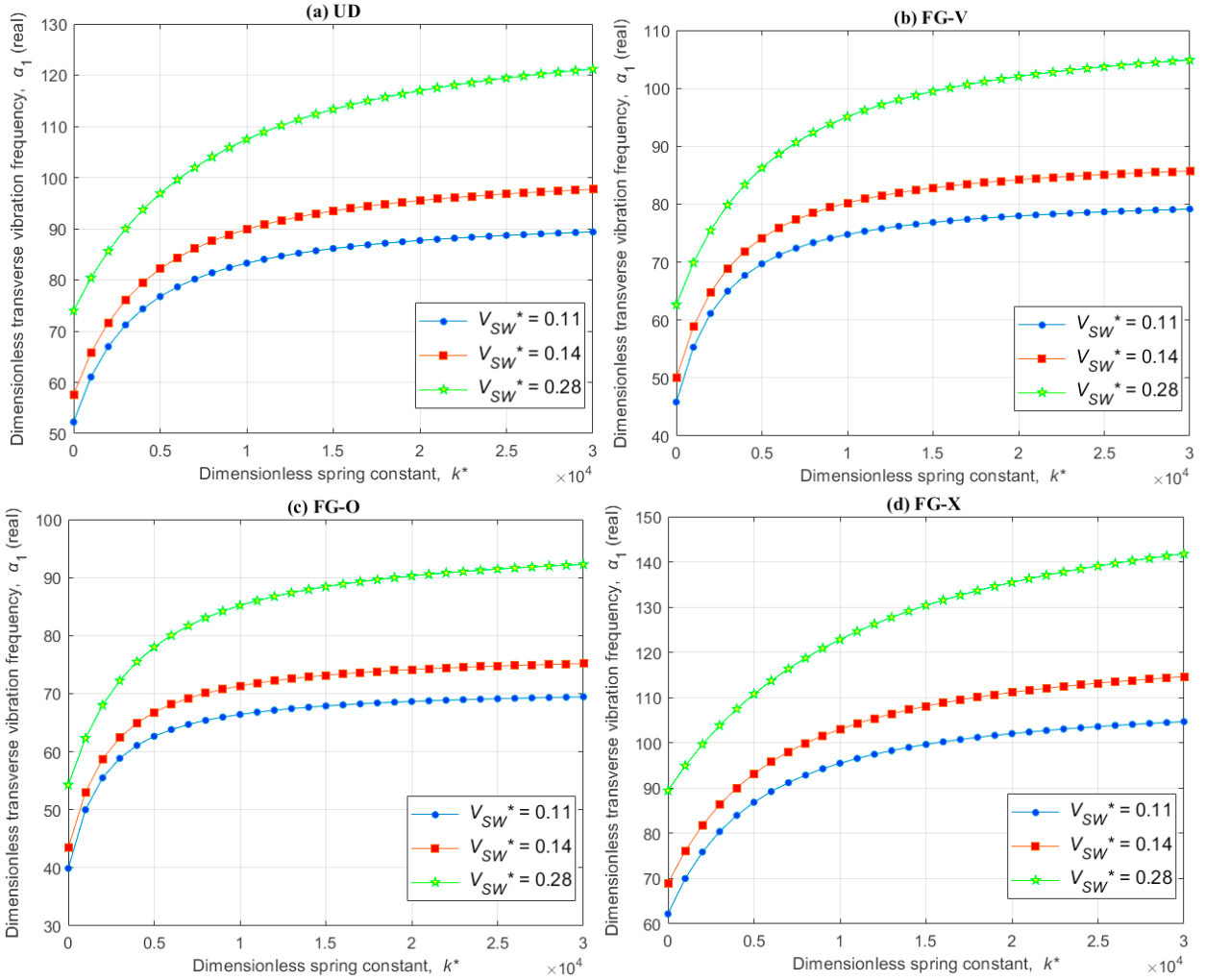

Fig. 2. Effects of increasing linear stiffness coefficient and CNT volume fraction on the real transverse natural frequency of axially travelling clamped-clamped beam with dimensionless axial speed, $c = 1$ for different FGCNT distributions: (a) UD, (b) FG-V, (c) FG-O, and (d) FG-X.

Fig. 2 shows the results for transverse vibration for the CNT reinforced clamped-clamped beam, with a dimensionless speed, c of 1. Three different volume fractions are considered with an increasing spring stiffness and constant axial speed. As the spring stiffness increases, the natural frequency increases. The addition of a spring support results in an initial spike in the natural frequency of the beam, then a linear increase for higher values of k. Fig. 2b, shows there is a similar trend to Fig. 2a; an increase in CNT volume fraction results in an increase in the transverse natural frequency of the beam. FG-V reinforcement has an overall lower natural frequency as opposed to a UD CNT reinforcement, for each of the respective reinforcement fractions. Fig. 2c illustrates the natural frequency of the axial

travelling beam with FG-O CNT reinforcement and an intermediate spring support. As per Fig. 2a & Fig. 2b, here is higher natural frequency for the same given spring stiffness. The overall natural frequencies for the FG-O beam are lower for the same spring stiffness when compared to UD & FG-V with the same volume fraction of CNT reinforcement. Fig. 2d shows the natural transverse frequency of the CNT reinforced beam with FG-X reinforcement. In addition, with an increase to the spring stiffness k, there is a higher natural frequency. Comparing the same reinforcement fraction and stiffness level from FG-X to the other types of reinforcement, yields the highest natural frequency of these configurations.

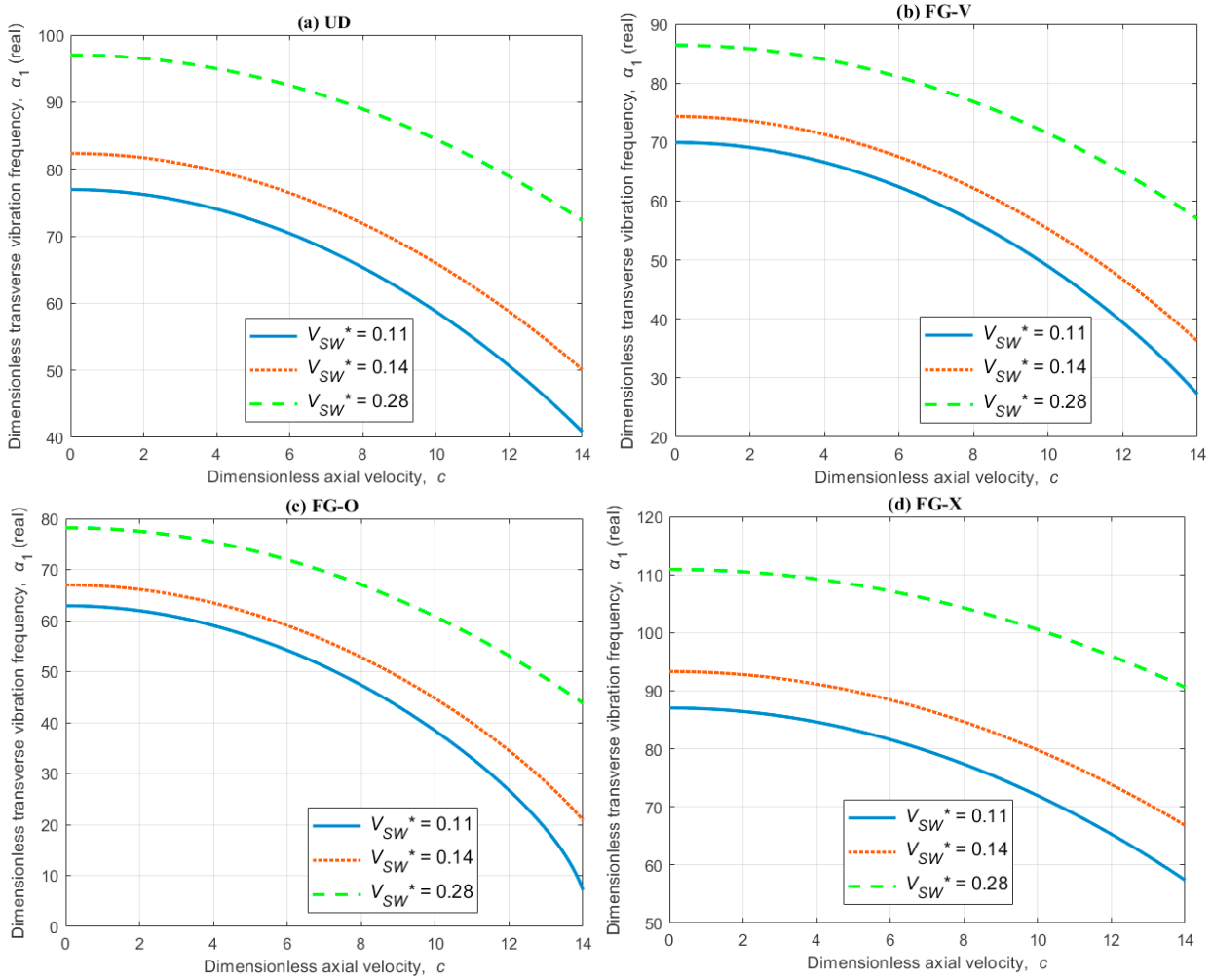

Fig. 3. Effects of increasing the dimensionless axial speed and CNT volume fraction on the real transverse natural frequency of a clamped-clamped beam with linear stiffness coefficient, $k^* = 5000$ for different FGCNT distributions: (a) UD, (b) FG-V, (c) FG-O, and (d) FG-X.

Fig. 3 shows that for all volume fractions of CNT reinforcement, as axial speed increases, the vibrational frequency of the beam decreases. In addition to a reduction in the beams' natural frequency, there is a sharper decline for higher dimensionless velocities. Fig. 3b exemplifies the natural frequency of an axially travelling beam with FG-V reinforcement, using the same setting as for the UD FGCNT. There is a lower natural frequency for FG-V compared to the same speed as the UD CNT reinforcement. Continuing with the same settings, only changing the FGCNT reinforcement profile to FG-O in Fig. 3c, yields a similar decrease in natural frequency when the dimensionless speed is increased. There is an overall lower natural frequency for all dimensionless velocities compared to both UD and FG-V reinforcements. FG-X reinforcement has the highest natural frequency for the same given dimensionless speed when compared to the other CNT reinforcements.

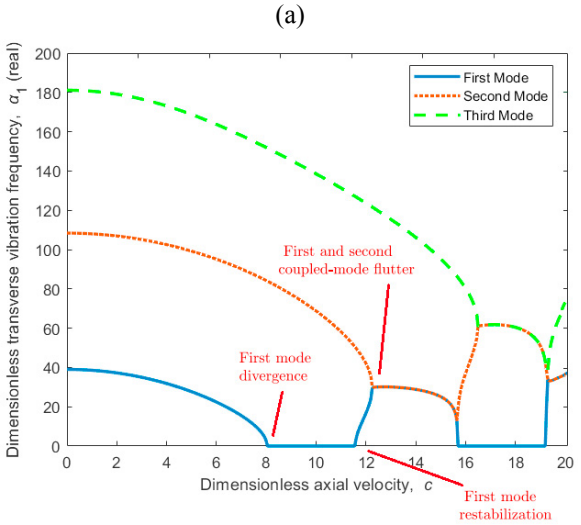

Fig. 4. (a) Real parts of the first three transverse vibrational frequencies of an axially travelling isotropic beam, versus the dimensionless axial velocity, c for linear spring stiffness $k^* = 10{,}000$.

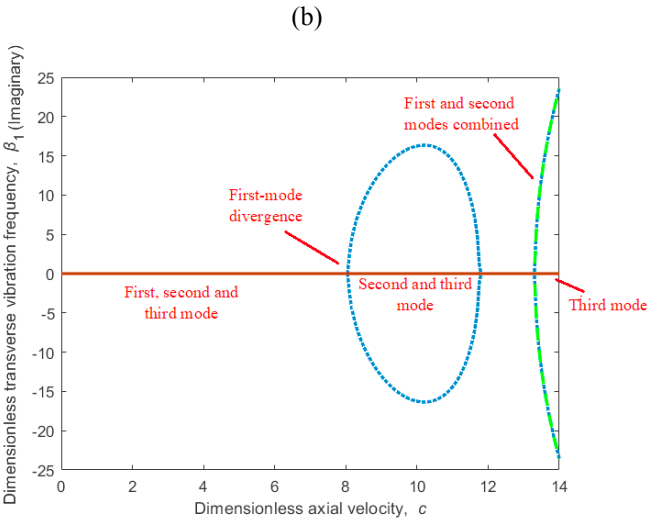

Fig. 4. (b) Imaginary parts of the first three transverse vibrational frequencies of an axially travelling isotropic beam, versus the dimensionless axial velocity, c for linear spring stiffness $k^* = 10{,}000$.

As shown in Fig. 4a and Fig. 4b, the real and imaginary parts respectively of the first three modes of vibration are compared to dimensionless axial velocity. Fig. 4a and Fig. 4b show that the only contribution to the vibration is from the real part, from when c is 0-8 dimensionless velocity. At 8, dimensionless velocity is the first occurrence of 0 natural frequency for both real and imaginary components; this is therefore the critical velocity. At this point of 0 natural frequency the system is no longer stable and has undergone the divergence phenomenon which is comparable to a beam undergoing a compressive load and then buckling. After this there is a divergence in the imaginary component for the first mode while the imaginary component of the second and third modes continue to not add to the transverse natural frequency. Following this loss in stability the natural frequency then rises. This is due to gyroscopic effects for higher dimensionless velocities. The system gains stability because of Coriolis force generating travelling waves in the system. From this, both Fig. 4a and Fig. 4b exemplifies the fact that divergence is directly related to the contribution, or lack of, from both the real and imaginary components. With a continued increase in the dimensionless velocity in the unstable part of the graph, the first natural frequency then rises, and the first mode restabilises, where there is a combination of the first and second frequencies when c is 12. Then, once there is a combination of the first and second real parts, there is a reduction in the natural frequency for any additional increase in the vibration. During this period there is no addition from the imaginary component. Increasing the axially velocity further begins to show instability, as the first real part of the natural frequency becomes 0. At this range there are also contributions from both first and second imaginary modes as they combine, when c is 14 dimensionless velocity.

5. Conclusion

This paper investigated the vibrational characteristics of axially travelling FGCNT reinforced Euler-Bernoulli beams under clamped-clamped boundary condition with an intermediate spring support. CNT distributions of UD, FG-V, FG-O and FG-X, have been considered for analysis. By utilising Hamilton's principle, the equations of motion were developed, and the natural frequencies were obtained via the modal decomposition technique. It is concluded that the introduction of CNT reinforcement has the result of increasing the transverse natural frequency. FG-O has the effect of increasing the natural frequency the least on the system when compared to all other reinforcement patterns, whereas FG-X has the highest increase to the transverse vibrational frequency. In all cases, increasing the spring stiffness increases the natural frequency for all beam reinforcement configurations, though to varying degrees for each of the CNT reinforcement configurations. All CNT reinforcement increases the natural frequency of the beam when compared to no CNT reinforcement at all, but when there is an increase to the speed of the axially travelling beam, it has the effect of lowering the natural frequency of all CNT when compared to no speed at all. Increasing the volume

fraction of CNT in the beam has the effect of increasing the natural frequency, but with an increase in speed the natural frequency reduces.

6. Acknowledgements

Thanks to Dr. Joseph Wayne Smith for his proof reading.

7. References

Ansari, R., Torabi, J., Hassani, R., 2019. A comprehensive study on the free vibration of arbitrary shaped thick functionally graded CNT-reinforced composite plates. Engineering Structures 181, 653-669.

Dahlberg, T., 2006. Moving force on an axially loaded beam—with applications to a railway overhead contact wire. Vehicle System Dynamics 44, 631-644.

Daikh, A.A., Houari, M.S.A., Belarbi, M.O., Chakraverty, S., Eltaher, M.A., 2022. Analysis of axially temperature-dependent functionally graded carbon nanotube reinforced composite plates. Engineering with Computers 38, 2533-2554.

Drissi-Habti, M., El Assami, Y., Raman, V., 2021. Multiscale toughening of composites with carbon nanotubes—continuous multiscale reinforcement new concept. Journal of Composites Science 5, pp. 135.

Farokhi, H., Ghayesh, M.H., Hussain, S., 2016. Three-dimensional nonlinear global dynamics of axially moving viscoelastic beams. Journal of Vibration and Acoustics 138, pp. 011007.

Iijima, S., Ichihashi, T., 1993. Single-shell carbon nanotubes of 1-nm diameter. Nature 363, 603-605.

Khaniki, H.B., Ghayesh, M.H., Hussain, S., Amabili, M., 2020. Porosity, mass and geometric imperfection sensitivity in coupled vibration characteristics of CNT-strengthened beams with different boundary conditions. Engineering with Computers 1-27.

Liew, K.M., Lei, Z.X., Zhang, L.W., 2015. Mechanical analysis of functionally graded carbon nanotube reinforced composites: a review. Composite Structures 120, 90-97.

Mohammadimehr, M., Monajemi, A.A., Afshari, H., 2020. Free and forced vibration analysis of viscoelastic damped FG-CNT reinforced micro composite beams. Microsystem Technologies 26, 3085-3099.

Ong, O.Z.S., Ghayesh, M.H., Losic, D., Amabili, M., 2022. Coupled dynamics of double beams reinforced with bidirectional functionally graded carbon nanotubes. Engineering Analysis with Boundary Elements 143, 263-282.

Öz, H.R., Pakdemirli, M., 1999. Vibrations of an axially moving beam with time-dependent velocity. Journal of Sound and Vibration 227, 239-257.

Öz, H.R., Pakdemirli, M., Boyacı, H., 2001. Non-linear vibrations and stability of an axially moving beam with time-dependent velocity. International Journal of Non-Linear Mechanics 36, 107-115.

Pakdemirli, M., Ulsoy, A.G., 1997. Stability analysis of an axially accelerating string. Journal of Sound and Vibration 203, 815-832.

Pellicano, F., Vestroni, F., 2002. Complex dynamics of high-speed axially moving systems. Journal of Sound and Vibration 258, 31-44.

Poornima, C., Mallik, U.S., Shivasiddaramaiah, A.G., Pushpalakshmi, N., Puneeth, B.S., 2021. Evaluation of wear characteristics of PP/MWCNT nanocomposites. Materials Today: Proceedings 46, 2477-2482.

Popov, V.N., 2004. Carbon nanotubes: properties and application. Materials Science and Engineering: R: Reports 43, 61-102.

Ravindra, B., Zhu, W.D., 1998. Low-dimensional chaotic response of axially accelerating continuum in the supercritical regime. Archive of Applied Mechanics 68, 195-205.

Shirasu, K., Nakamura, A., Yamamoto, G., Ogasawara, T., Shimamura, Y., Inoue, Y., Hashida, T., 2017. Potential use of CNTs for production of zero thermal expansion coefficient composite materials: An experimental evaluation of axial thermal expansion coefficient of CNTs using a combination of thermal expansion and uniaxial tensile tests. Composites Part A: Applied Science and Manufacturing 95, 152-160.

Swanson, E., Powell, C.D., Weissman, S., 2005. A practical review of rotating machinery critical speeds and modes. Sound and Vibration 39, 16-17.

Thomas, B., Roy, T., 2016. Vibration analysis of functionally graded carbon nanotube-reinforced composite shell structures. Acta Mechanica 227, 581-599.

Wattanasakulpong, N., Chaikittiratana, A., 2015. Flexural vibration of imperfect functionally graded beams based on Timoshenko beam theory: Chebyshev collocation method. Meccanica 50, 1331-1342.

Yan, T., Yang, T., Chen, L., 2020. Direct multiscale analysis of stability of an axially moving functionally graded beam with time-dependent velocity. Acta Mechanica Solida Sinica 33, 150-163.

Yang, X.D., Chen, L.Q., 2005. Bifurcation and chaos of an axially accelerating viscoelastic beam. Chaos, Solitons & Fractals 23, 249-258.

Zafar, U.S.M.A.N., 2018. Literature review of wind turbines. Chair of Geotechnical Engineering Bauhaus Universität, Weimar.

Zhai, W., Bai, L., Zhou, R., Fan, X., Kang, G., Liu, Y., Zhou, K., 2021. Recent progress on wear-resistant materials: designs, properties, and applications. Advanced Science 8, pp.2003739.